Hindawi
Advances in Materials Science and Engineering
Volume 2018, Article ID 7531912, 13 pages
https://doi.org/10.1155/2018/7531912

Research Article

Experimental Study and Mixed-Dimensional FE Analysis of T-Rib GFRP Plate-Concrete Composite Bridge Decks

Jun Tian,[1] Xiaowei Wu,[1] Yu Zheng,[1] Yinfei Du,[2] and Xiankai Quan[2]

[1]*School of Environment and Civil Engineering, Dongguan University of Technology, Dongguan 523808, China*
[2]*School of Civil Engineering, Central South University, Changsha 410075, China*

Correspondence should be addressed to Xiaowei Wu; wxw1014aa@163.com

Received 26 May 2018; Accepted 27 August 2018; Published 25 September 2018

Academic Editor: Aniello Riccio

In order to extend the understanding of structural performance of a T-rib glass fibre-reinforced polymer (GFRP) plate-concrete composite bridge deck, four GFRP plate-concrete composite bridge decks were tested, which consist of cast-in-place concrete sitting on a GFRP plate with T-ribs. Subsequently, a mixed-dimensional finite element (FE) analysis model was proposed to simulate the behavior of the test models. The test and simulation results showed that the composite specimens had an excellent interface bonding performance between GFRP plate and concrete throughout flexural response until specimens failure occurred. The failure mode of those composite specimens was shear failure in concrete structures. It was found that the interface roughness of the GFRP plate could not affect the ultimate bearing capacity and stiffness of composite specimens significantly. However, the height of concrete structures had a strong effect on those structural behaviors. In addition, the longitudinal compressive reinforcing CFRP rebars had a little influence on ultimate bearing capacity of composite specimens, while it had a significant influence on ductility of composite specimens. The mixed-dimensional FE analysis model can accurately simulate the local complex stress state of GFRP plates, ultimate loads, stiffness, and midspan deflections and simultaneously can significantly reduce computational time. Therefore, mixed-dimensional FE analysis can provide a suitable solution to simulate the structural performance of T-rib GFRP plate-concrete composite bridge decks.

1. Introduction

Compared with the FRP structure, the FRP-concrete composite/hybrid structures have more advantages, such as preventing the buckling phenomena of pultruded FRP profiles [1, 2], improving the usage of FRP profiles strength [3], reducing material costs [4], and improving stability, flexural stiffness, and bearing capacity of structures [5]. Furthermore, the FRP profiles/plates can act as a temporary formwork when pouring the cast-in-place concrete [6]. Hence, the application of FRP-concrete composite bridge decks becomes more and more widespread in recent years [7–14].

Researchers proposed some FRP-concrete composite structures with different shapes of cross sections, such as a rectangular [15–17], box [18, 19], or I-shape section [8, 20–22], as shown in Figure 1. The failure modes of these composite structures are primarily interface bonding failure between FRP profiles/plates and concrete [23–29]. The material strength of these composite structures cannot be effectively used due to interface bonding failure. Therefore, increasing the bonding behaviors between FRP profiles/plates and concrete is significantly critical for these structures.

In order to obtain an improved interface bonding performance between FRP profiles/plates and concrete, some composite structures with different shapes of cross sections were proposed, as shown in Figure 2(a) [30], Figure 2(b) [31], and Figure 2(c) [32]. In addition, a T-rib glass fibre-reinforced polymer (GFRP) plate-concrete composite bridge deck was also proposed in this paper, which consists of cast-in-place concrete sitting on a GFRP plate with T-ribs, as shown in Figure 2(d).

The finite element method (FEM) is widely used to analyse the structural performance of FRP-concrete composite structures, due to the better accuracy and feasibility of

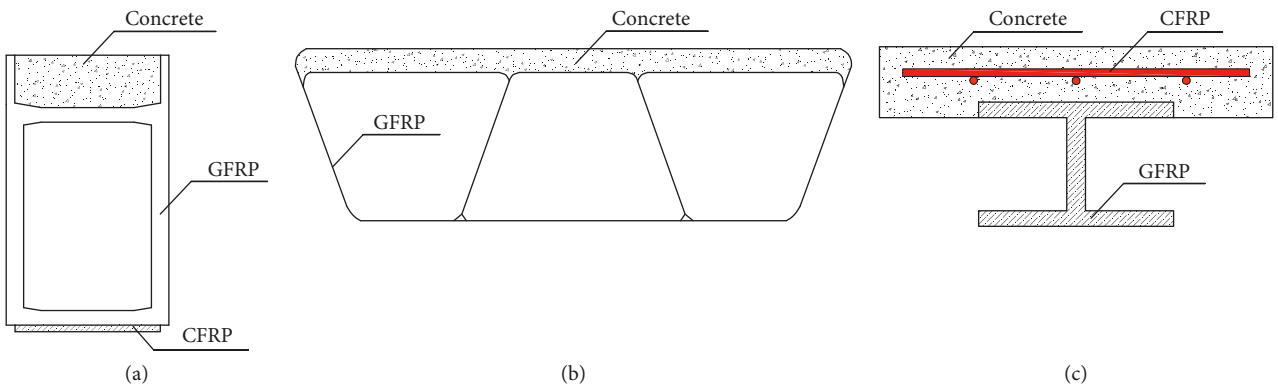

Figure 1: FRP-concrete composite decks with different sections: (a) rectangular section; (b) box section; (c) I-shape section.

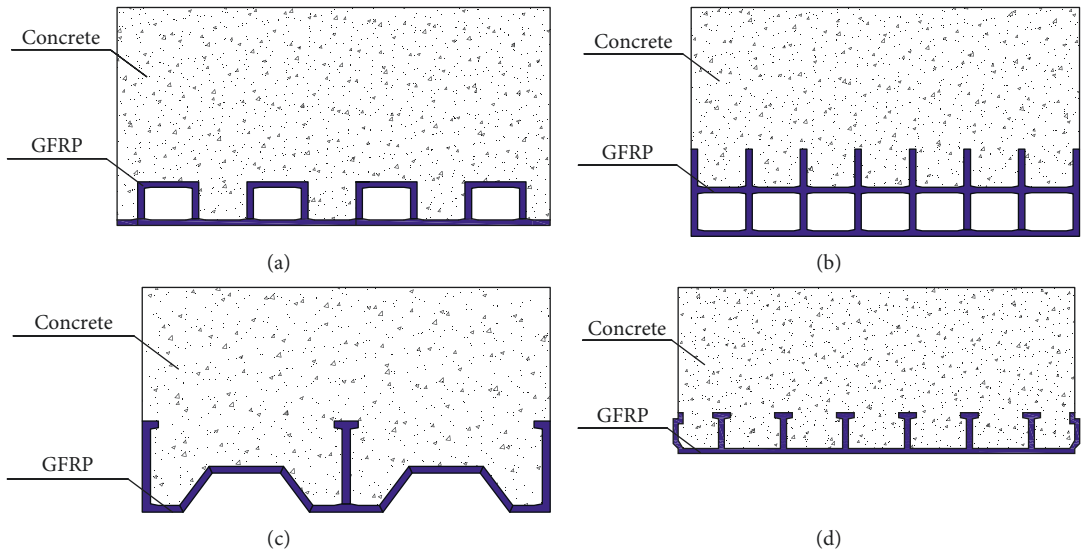

Figure 2: GFRP-concrete composite decks with different sections: (a) Type I; (b) Type II; (c) Type III; (d) Type IV.

FEM than the other analysis methods (e.g., Euler–Bernoulli beam theory [33], Timoshenko beam theory [3, 15, 21, 34], and orthotropic plate theory [4]). According to element types used in simulation composite structures, the FEA model can be divided into three types, namely, FEA model with truss elements, shell elements, and solid elements, respectively. (1) The FEA model with truss elements was the two-dimensional truss elements adopted to simulate FRP profiles/plates and concrete [35]. (2) The FEA model with shell elements was the two-dimensional shell elements and three-dimensional solid elements adopted to simulate FRP profiles/plates and concrete [3, 4, 8, 15, 22, 36–38], respectively. (3) The FEA model with solid elements was the three-dimensional solid elements adopted to simulate concrete and FRP profiles/plates [34, 39–41].

The FEA model with truss elements and shell elements is unable to simulate the stress state of FRP profiles/plates along the thickness direction and also unable to simulate the three-dimensional stress state of FRP profiles/plates (e.g., box section, rectangular section, and I-shape section) at the intersection or near the T-ribs. By contrast, though the FEA model with solid elements can overcome the above deficiency, the computational time is very long and computational efficiency is very low.

As a result, the flexural experiments on the proposed T-rib GFRP plate-concrete composite bridge decks in this paper were performed to examine the feasibility and in-depth understanding of structural performance. Furthermore, a mixed-dimensional FEA model is proposed for high efficiency analysis of the GFRP plate-concrete composite bridge deck and accurately simulating the local complex stress state of GFRP plates.

2. Experimental Program

2.1. Description of Specimens. A total of four rectangular GFRP-concrete composite bridge decks were designed and conducted. The GFRP plate was used to carry tensile force, and the cast-in-place concrete was poured on the upper surface of the GFRP plate to carry compressive force. The details, including geometric dimensions and test parameters, of all specimens used in the test are shown in Table 1.

Table 1: Details of all specimens.

Specimens	Width and length of the specimens (mm × mm)	Height of the specimens (mm)	Interface types	Reinforcement CFRP rebars
GC-1	305 × 1300	200	Type I	—
GC-2	305 × 1300	200	Type II	—
GC-3	305 × 1300	150	Type I	—
GC-4	305 × 1300	200	Type I	CFRP rebars in the compressive zone

For the convenience of the experiment, the pultruded GFRP plate was halved according to the symmetry of the structure. Then, the halved GFRP plate with five T-type ribs and one special-shaped rib is shown in Figure 3(a). The specimens GC-1, GC-2, and GC-4 had identical geometric dimensions of 305 mm in width, 200 mm in height, and 1300 mm in length; while specimen GC-3 had a same geometric dimension in width and length, expect the 150 mm height, as shown in Figures 3(b) and 3(c).

To investigate the effect of CFRP rebars on the structural performance of composite specimens, two 8 mm diameter CFRP rebars were placed in the compressive zone of the composite specimen as the longitudinal compressive reinforcement. Moreover, the horizontal CFRP rebars spacing at 165 mm center to center were tied with two longitudinal CFRP rebars at the intersections to form a reinforcement mesh, as shown in Figure 3(c).

Two types of interfaces (i.e., type I and type II) were generated by treating the GFRP plate surface bonded with cast-in-place concrete. The interface of specimens coded as GC-1, GC-3, and GC-4 was interface type I, while interface type II was used in specimen GC-2.

The interface type I was that the 2 mm even thick epoxy brushed onto the GFRP plate, 2–5 mm aggregates immediately spread onto the epoxy resin, and then the rough interface of the GFRP plate formed. The type II interface was the concrete placed directly against the GFRP plate. A set of the device, which consisted of a dial indicator and flat base, was designed to measure the interface roughness, as shown in Figure 4. The average value of the vertical height difference between protruding and concave portions of the interface was used to quantitatively assess the interface roughness [42]. The measured interface roughness values of type I was 3.33 mm.

The manufacturing process of all composite specimens is described in detail as follows: the GFRP plate acts as the bottom formwork of the composite specimen and four wooden boards as the side formwork. For specimens GC-1, GC-3, and GC-4 with the interface type I, the interface was manufactured according to the abovementioned method. According to previous research results conducted by Zhang et al. [43], the best initial placement time of cast-in-place concrete onto the adhesive resin-coated GFRP plate is about 30 minutes. So, after 30 minutes curing of the adhesive layer, the cast-in-place concrete was poured into the moulds against the adhesive layer to form the composite specimens. For specimen GC-2 with the type II interface, the cast-in-place concrete was directly poured into the moulds to form the composite specimen after cleaning of the GFRP plate. All the specimens were cured under the temperature of 20 ± 2°C and humidity of 95% for 28 days.

2.2. Material Properties. Ordinary Portland cement (CEM I 42.5N) was used for the cast-in-place concrete. The fine aggregate was natural sand with sizes below 1.7 mm, and the coarse aggregate was crushed limestone with sizes between 5 mm and 20 mm. The polycarboxylic-based water-reducing agent produced by Subote New Material Co., Ltd of China was used to obtain good workability. The mass ratio of the cast-in-place concrete was 1 (cement) : 0.39 (water) : 1.06 (fine aggregate) : 2.72 (coarse aggregate) : 0.0075 (water-reducing agent). The measured average compressive strength, tensile strength, and elastic modulus of the cast-in-place concrete were 34.6 MPa, 2.2 MPa, and 31.4 GPa, respectively, according to the methods reported in GB/T 50081-2002 [44].

The GFRP plate and CFRP rebar were all produced by Nanjing Hitech Composites Co., Ltd of China. Sikadur-330 epoxy resin was produced by Sika Corporation of Switzerland. Material parameters of the GFRP plate, CFRP rebar, and Sikadur-330 epoxy resin were provided by the manufacturers. The ultimate tensile strength, tensile elastic modulus, and elongation of the GFRP plate were 471 MPa, 26.6 GPa, and 1.9%, respectively. The ultimate tension strength, elastic modulus, and elongation of the CFRP rebars were 2100 MPa, 147 GPa, and 1.5%, respectively. The ultimate tension strength, elastic modulus, and elongation of Sikadur-330 epoxy resin were 30 MPa, 3.8 GPa, and 1.6%, respectively. A summary of material properties is shown in Table 2.

2.3. Experimental Setup and Instrumentations. The experimental setup is shown in Figure 5. All specimens were simply supported on two rollers spaced at 1000 mm. And all specimens were applied in four-point bending under monotonically increasing loads, through a 350 kN capacity hydraulic jack. The whole loading process was controlled at a speed of 0.5 mm/min. The load values were determined through a load cell between the jack and the reaction frame.

A fully instrumented specimen is also shown in Figure 5. Three linear variable displacement transducers (LVDTs) were applied to measure deflection of midspan and two supporting points. Five 100 mm long strain gauges on the specimen side were applied to measure strain distributions at midspan cross section.

2.4. Test Results and Discussion

2.4.1. Failure Mode and Characteristics Data. Detailed test phenomena of all specimens under monotonically increasing load are described as follows: for the specimens GC-1, GC-2, GC-3, and GC-4, when applied loads of 55 kN, 50 kN, 40 kN, and 55 kN, respectively, the first microcrack

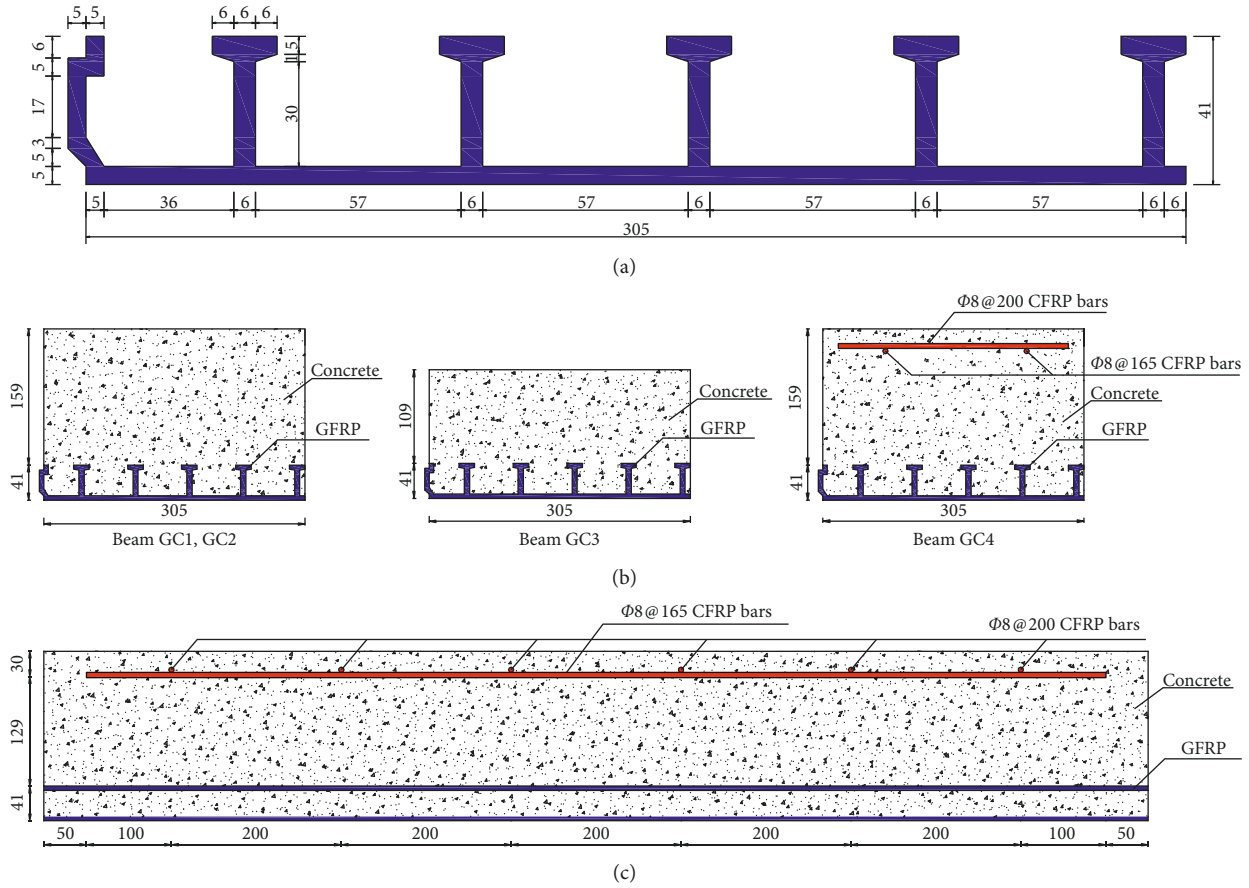

Figure 3: Design of all test specimens (mm): (a) details of the GFRP plate; (b) cross section of all test specimens; (c) elevation view of specimen GC-4.

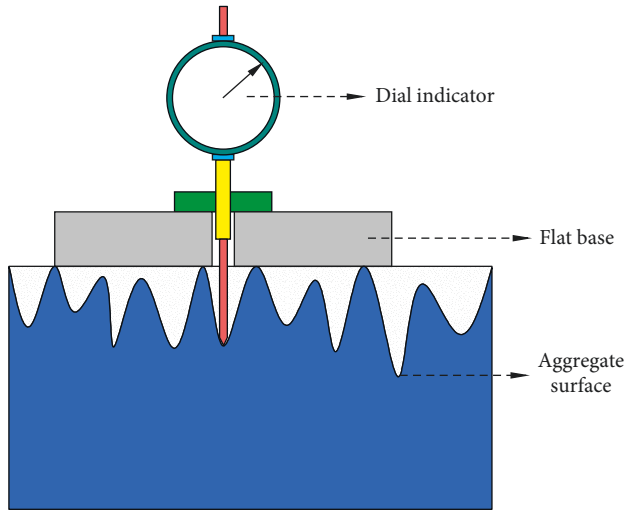

Figure 4: Measurement principle of interface roughness.

was found at the bottom of the concrete. And then with the increasing loads, the first microcrack widened and extended upward, and the new cracks also formed. For instance, the cracks distribution of specimen GC-2 is shown in Figure 6 (not all are shown here for brevity).

For the specimens GC-1, GC-2, GC-3, and GC-4, when applied loads beyond 80 kN, 200 kN, 180 kN, and 200 kN, respectively, the specimens began to make a continuous noise in the process of increasing loads. When the applied loads were 242.3 kN, 226.3 kN, 192.5 kN, and 267.1 kN, respectively, the shear failure of concrete occurred (diagonal racks through concrete cross section), while the concrete remained better bonded to the GFRP plates/T-ribs, and there was almost no slip between the concrete and GFRP plate throughout the flexural response until concrete shear failure occurred. For instance, the failure mode of specimen GC-3 is shown in Figure 7 (not all are shown here for brevity).

The test results, including crack load, ultimate load, midspan deflection at the ultimate load, ultimate relative slip between GFRP plate and concrete, and failure mode, of all specimens are shown in Table 3.

It can be found that failure mode of all specimens was concrete shear failure and there was almost no slip between the concrete and GFRP plate, indicating that the interface roughness of the GFRP plate, the height of concrete cross section, and the longitudinal compressive reinforcing CFRP rebars had no influence on the failure mode of the composite specimens.

Table 2: Summary of material properties.

Material	Strength (MPa)		Elastic modulus (GPa)			Poisson's ratio			Elongation (%)	Density (kg/m^3)
	Compression	Tension	X	Y	Z	XY	YZ	XZ		
Concrete	34.6	2.2	31.4	—	—	0.2	—	—	—	2600
GFRP	—	471	26.6	13.6	13.6	0.3	0.3	0.2	1.9	2000
CFRP rebar	—	2100	147	—	—	0.3	—	—	1.5	1600
Adhesive resin	—	30	3.8	—	—	0.38	—	—	1.6	1310

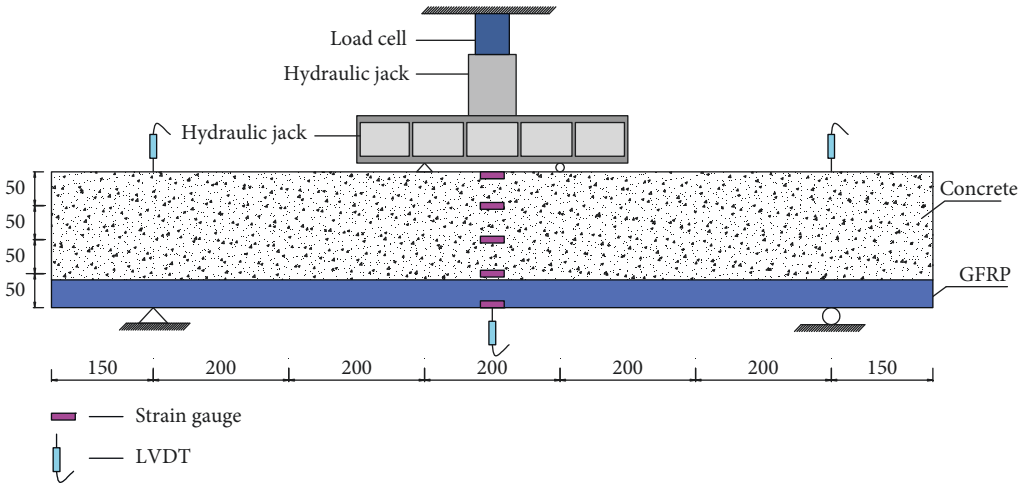

Figure 5: Experimental setup (mm).

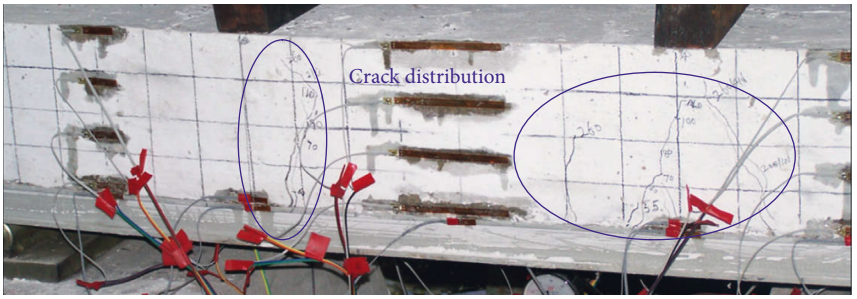

Figure 6: Specimen GC-2 cracks distribution before concrete shear failure.

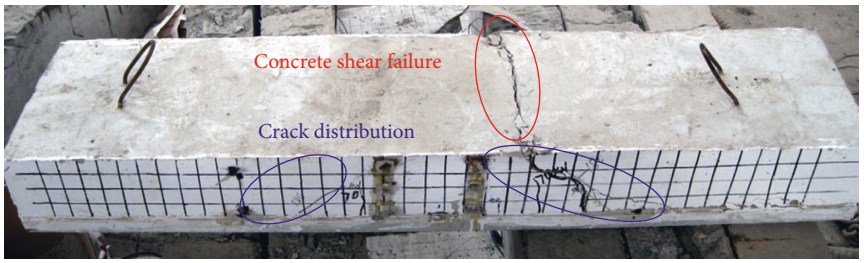

Figure 7: Specimen GC-3 cracks distribution and failure mode.

It can also be seen that the crack loads of specimens GC-2 and GC-3 were 9% and 27% lower than that of specimen GC-1, respectively, while the crack load of specimens GC-1 and GC-4 was identical, indicating that the interface roughness of the GFRP plate and height of concrete cross section had a significant influence on crack loads, while the longitudinal compressive reinforcing the CFRP rebars had almost no influence on crack loads.

2.4.2. Load-Deflection Curve at Midspan Cross Section. The load-deflection curves of all specimens at the midspan section are shown in Figure 8. It can be found that variations

Table 3: Test data summary.

Beam	Crack load (kN)	Ultimate load (kN)	Midspan deflection at the ultimate load (mm)	Ultimate relative slip (mm)	Failure mode
GC-1	55.0	242.3	3.15	0	Concrete shear failure
GC-2	50.0	226.3	3.17	0	Concrete shear failure
GC-3	40.0	192.5	4.10	0	Concrete shear failure
GC-4	55.0	267.1	4.09	0	Concrete shear failure

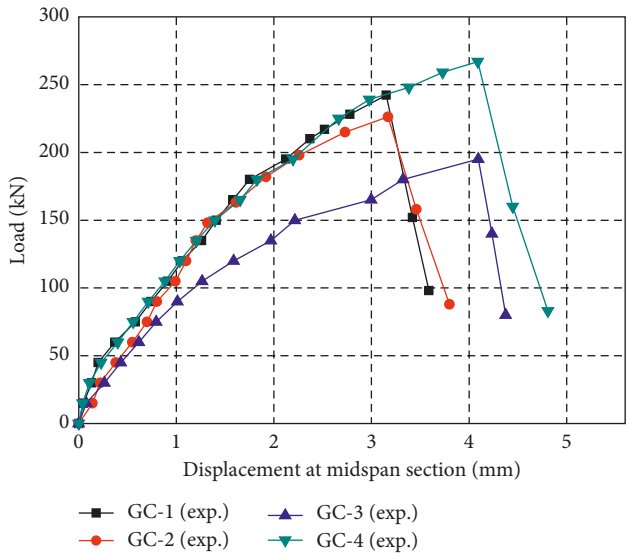

Figure 8: Comparison of experimental load-deflection curves at midspan cross section.

of load-deflection curves of specimens were basically similar. Before ultimate loads of 70%, the load-deflection curves of all specimens were linear. Hereafter, the stiffness of all specimens decreased slightly, and the load-displacement curves showed nonlinearity. After the ultimate loads, the load-displacement curves presented a sharp decline because the shear failure of concrete occurred.

By comparing the load-deflection curves of specimens GC-1 and GC-2, it can be found that, before the ultimate load of 70%, the stiffness of specimens GC-1 and GC-4 was basically identical. Hereafter, the stiffness of specimen GC-2 was slightly lower than that of specimens GC-1, and the ultimate load of specimen GC-2 was also 6.6% lower than that of specimen GC-1. It can be concluded that the interface roughness of the GFPR plate had a slight influence on the ultimate bearing capacity and stiffness of composite specimens.

By comparing the load-deflection curves of specimens GC-1 and GC-3, it can be found that the stiffness of specimen GC-3 was significantly lower than that of specimen GC-1, and the ultimate load of specimen GC-3 was also 20.6% lower than that of specimen GC-1. It can be concluded that the height of concrete cross section had a significant influence on ultimate bearing capacity and stiffness of composite specimens.

By comparing the load-deflection curves of specimens GC-1 and GC-4, it can be found that the stiffness of specimens GC-1 and GC-4 was basically identical before the ultimate loads of composite specimens. However, the ultimate load of specimen GC-4 was 10.2% higher than that of specimen GC-1, and the midspan deflection of specimen GC-4 at the ultimate load was 29.8% higher than that of specimen GC-1. It might be explained by the fact that the concrete shear failure of composite specimens was delayed because the CFRP bars restricted development of concrete cracks and assisted the concrete to bear compressive stress. Therefore, it can be concluded that the longitudinal compressive reinforcing CFRP rebars had a little influence on ultimate bearing capacity while had a significant influence on ductility of composite specimens.

2.4.3. Strain Distributions at Midspan Cross Section. The strain distribution at midspan cross section of all specimens is shown in Figure 9. In Figure 9, P_u indicates the ultimate load of the specimens, and the height of cross section is zero at the bottom of the GFRP plates. It can be found that the strain distributions of all specimens were generally linear, and there was almost no strain redistribution caused by the interface slip. Combining the test results of the relative slip between the concrete and GFRP plate (Table 3), it can be concluded that the T-rib GFRP plate-concrete composite bridge deck proposed in this paper had an excellent interface bonding performance between GFRP plate and concrete throughout the flexural response until concrete shear failure occurred.

3. Finite Element Analysis of Mixed-Dimensional Model

3.1. Constitutive Modeling and Failure Criterion. Before FE analysis of the GFRP plate-concrete composite specimens, some assumptions of the constitutive models and failure criterions of all materials were made for simplicity.

(1) Subjected to the tensile force, the stress-strain relationship of concrete is linear before ultimate tensile strain ε_{tu}. Subjected to the pressure force, the stress-strain relationship of concrete is a quadratic parabola before the compressive strength f_c and then keeps a constant value until ultimate pressure strain ε_{cu}; the stress-strain curve of concrete is as shown in Figure 10(a), and the stress-strain equation of concrete is as shown in Equation (1). In Equation (1), the ultimate tensile strain ε_{tu}, peak stress pressure strain ε_0, and ultimate pressure strain ε_{cu} are −0.00007, 0.002, and 0.0033, respectively:

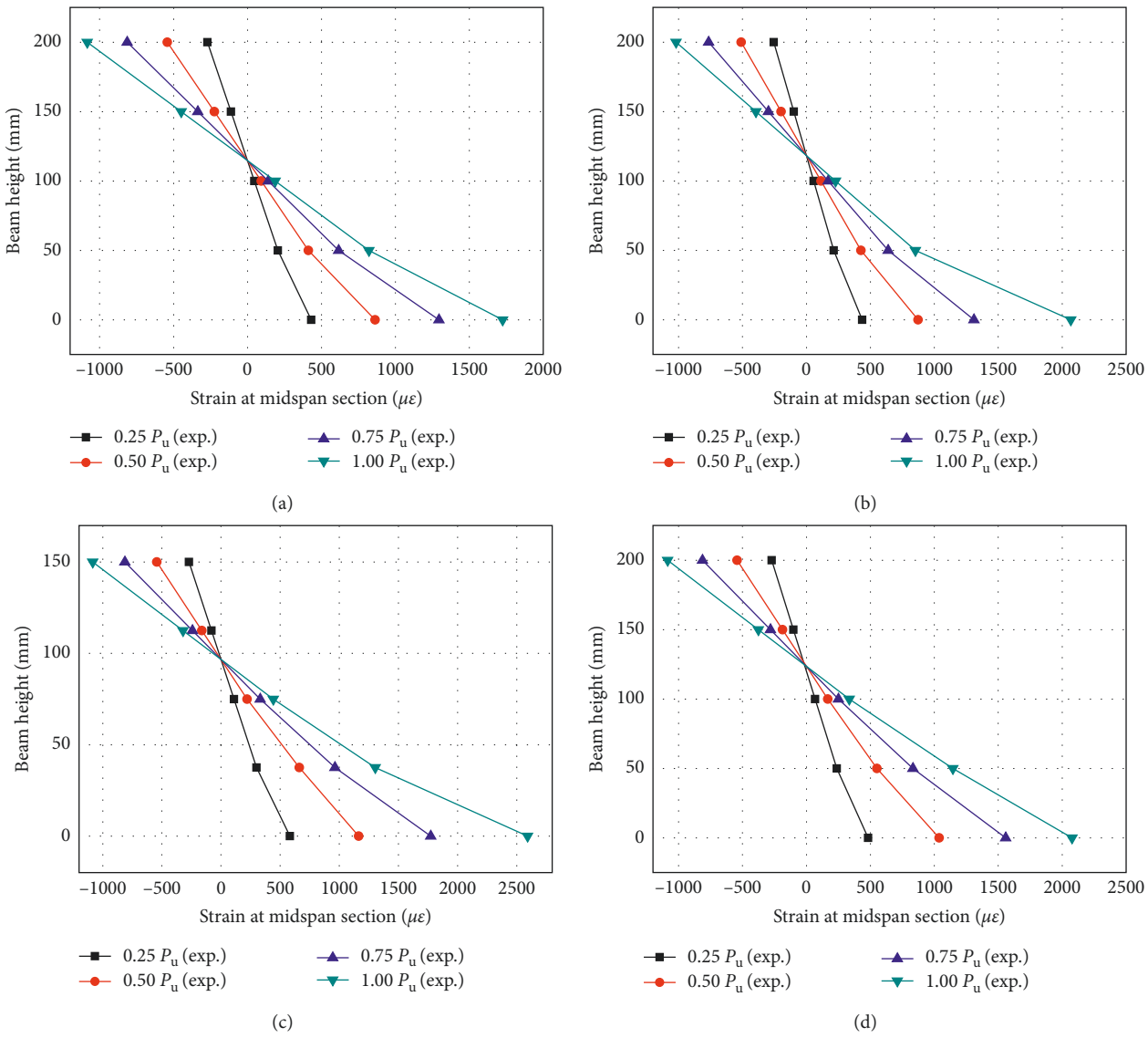

Figure 9: Strain distribution at the midspan cross section: (a) specimen GC-1; (b) specimen GC-2; (c) specimen GC-3; (d) specimen GC-4.

$$\sigma_c = \begin{cases} E_c\varepsilon, & \varepsilon_{tu} \le \varepsilon < 0, \\ f_c\left[\dfrac{2\varepsilon}{\varepsilon_0} - \left(\dfrac{\varepsilon}{\varepsilon_0}\right)^2\right], & 0 \le \varepsilon < \varepsilon_0, \\ f_c, & \varepsilon_0 \le \varepsilon \le \varepsilon_{cu}. \end{cases} \quad (1)$$

(2) The stress-strain relationship of the GFRP plate and CFRP rebar is all linear, and the stress-strain curves of the GFRP plate and CFRP rebar are as shown in Figures 10(b) and 10(c), respectively. And the stress-strain equations of the GFRP plate and CFRP rebar are shown in Equations (2) and (3), respectively. In Equations (2) and (3), the ultimate tensile strain of the GFRP plate ε_{ugf} and ultimate pressure strain of the CFRP rebar ε_{ucf} are 0.0177 and 0.002, respectively:

$$\sigma_{gf} = E_{f1}\varepsilon, \quad 0 \le \varepsilon \le \varepsilon_{ugf}, \quad (2)$$

$$\sigma_{cf} = E_{f2}\varepsilon, \quad 0 \le \varepsilon \le \varepsilon_{ucf}. \quad (3)$$

(3) The failure criterion of concrete is the five-parameter Willam–Warnke failure criterion. The failure criterions of the GFRP plate and CFRP rebar are that the tensile strain and pressure strain reached ultimate tensile strain ε_{ugf} and ultimate pressure strain ε_{ucf}, respectively.

3.2. GFRP-Concrete Interface. The experimental results of this paper showed that the T-rib GFRP plate-concrete composite specimens with an excellent interface bond

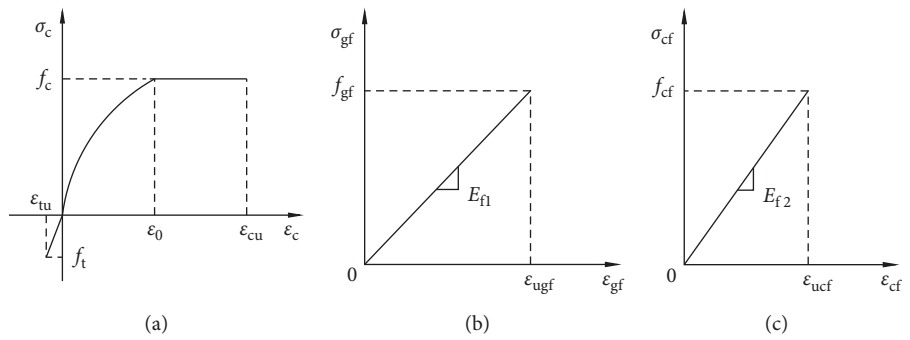

Figure 10: Stress-strain curve of all materials: (a) stress-strain curve of concrete; (b) stress-strain curve of the GFRP plate; (c) stress-strain curve of the CFRP rebar.

between concrete and GFRP plate and the insignificant or almost no slip between the concrete and GFRP plate throughout the flexural response until concrete shear failure occurred. Moreover, the destruction of composite specimens with type I and II interface was all determined by the concrete (i.e., shear failure of concrete). As a result, a bond-slip criterion between the GFRP plate and concrete was not necessary, and assume a perfect bond between GFRP plate and concrete.

3.3. Interface Coupling of Solid and Shell Elements in the Mixed-Dimensional Model. Since different types of solid element and shell element have different numbers of degrees-of-freedom (DOFs), the mixed-dimensional FE model needs a rational FE coupling method to combine mixed-dimensional finite elements at their interfaces into a single FE model. The constraint equations can be used to establish the interface coupling for elements of different DOFs [45].

The relationship between solid element and shell element at the coupling interface is shown in Figure 11. At the coupling interface, the solid elements nodes are 1, 2, and 3, respectively, while the shell element node is only $2'$. In the global coordinate system, displacement parameters of solid elements nodes 1, 2, and 3 are $u_1, v_1, w_1, u_2, v_2, w_2, u_3, v_3$, and w_3, respectively, while the displacement parameters of shell elements node $2'$ are $u_{2'}, v_{2'}, w_{2'}, \alpha_{2'}$, and $\beta_{2'}$, respectively.

The displacement parameters of nodes at the coupling interface are transferred from the global coordinate system to the local coordinate system according to the following equation:

$$\begin{pmatrix} u_i^* \\ v_i^* \\ w_i^* \end{pmatrix} = \lambda^T \begin{pmatrix} u_i \\ v_i \\ w_i \end{pmatrix}, \quad (i = 1, 2, 3), \tag{4}$$

$$\lambda = \begin{bmatrix} l_{1i} & l_{2i} & l_{3i} \\ m_{1i} & m_{2i} & m_{2i} \\ n_{1i} & n_{2i} & n_{3i} \end{bmatrix}, \quad (i = 1, 2, 3). \tag{5}$$

In Equation (4), the u_i^*, v_i^*, and w_i^* are nodes displacement components along the x-axis, y-axis, and z-axis in the local coordinate system, respectively. The u_i, v_i, and w_i are nodes displacement components along the x-axis, y-axis, and z-axis in the global coordinate system, respectively.

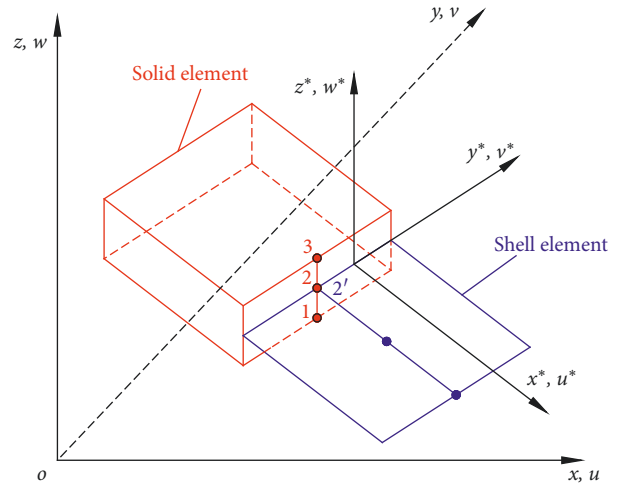

Figure 11: Relationship of solid elements and shell elements at the coupling interface.

In order to achieve displacement compatibility at the coupling interface, the constraint equations were used to establish the interface coupling for solid elements and shell elements in the local coordinate system [46], as shown in following equations, respectively:

$$\begin{aligned} u_2^* &= u_{2'}^*, \\ v_2^* &= v_{2'}^*, \\ w_2^* &= w_{2'}^*, \end{aligned} \tag{6}$$

$$\begin{aligned} u_2^* &= \frac{u_1^* + u_3^*}{2}, \\ v_2^* &= \frac{v_1^* + v_3^*}{2}, \\ w_2^* &= \frac{w_1^* + w_3^*}{2}, \end{aligned} \tag{7}$$

$$\alpha_{2'} = \frac{u_1^* - u_3^*}{t},$$
$$\beta_{2'} = \frac{v_3^* - v_1^*}{t}. \tag{8}$$

The above formulas can also be rewritten as follows:

$$C = \begin{pmatrix} u_2 - u_{2'} \\ v_2 - v_{2'} \\ w_2 - w_{2'} \\ u_2^* - \dfrac{u_1^* + u_3^*}{2} \\ v_2^* - \dfrac{v_1^* + v_3^*}{2} \\ w_2^* - \dfrac{w_1^* + w_3^*}{2} \\ \alpha_{2'} - \dfrac{u_1^* - u_3^*}{t} \\ \beta_{2'} - \dfrac{v_3^* - v_1^*}{t} \end{pmatrix} = 0. \tag{9}$$

Equation (9) is the constraint equations of solid elements and shell elements in the coupling interface.

3.4. Mixed-Dimensional Model. The commercial software ANSYS was applied to facilitate the mixed-dimensional FE analysis of T-rib GFRP plate-concrete composite bridge decks. A mixed-dimensional FE model was proposed for high efficiency analysis of the GFRP plate-concrete composite bridge deck and accurately simulating the local complex stress state of GFRP plates. In the model, three-dimensional solid elements were adopted to simulate concrete, while two-dimensional shell elements and three-dimensional solid elements were simultaneously adopted to simulate the GFRP plate. The section of T-ribs and GFRP plates at the intersection under the relatively complex stress state was simulated using three-dimensional solid elements, while the rest of the section under the relatively simple stress state was simulated using two-dimensional shell elements.

The specimen GC-1 as the research object and the relevant material parameters of the GFRP plate and concrete are listed in Table 1. For comparison purposes, three FE models with different methods were established. (1) Model I: GFRP plates/T-ribs were simulated using shell 63 elements, and concrete was simulated using solid 65 elements, as shown in Figure 12(a); (2) Model II: GFRP plates/T-ribs were simulated using solid 64 elements, and concrete was simulated using solid 65 elements, as shown in Figure 12(b); and (3) Model III: GFRP plates at the intersection and T-ribs were simulated using solid 64 elements, while the rest of the section was simulated using shell 63 elements, and concrete was simulated using solid 65 elements, as shown in Figure 12(c). The FEA method of the mixed-dimensional model (i.e., Model III) was named the mixed elements method for brevity in this paper.

The constraint equation of Equation (9) in this paper was used to establish the interface coupling for shell 63 elements and solid 64 elements. The shell element nodes were used as main nodes, while the solid element nodes are used as attached nodes. The DOFs of main nodes in all three directions (i.e., X, Y, and Z directions) were coupled, as shown in Figure 12(d).

The comparisons of the three different FE modes are shown in Table 4. Model I had the minimum total number of elements and the shortest computational time; however, the two-dimensional shell elements are unable to simulate the stress state of GFRP plates along the thickness direction and unable to simulate the three-dimensional stress state of GFRP plates at the intersection or near the T-ribs. Although Model II could overcome the above deficiency, it had the maximum total number of elements and the longest computational time. Model III could significantly decrease the total number of elements and the computational time as compared to that of Model II, but it still could simulate the stress state of GFRP plates along the thickness direction and simulate the three-dimensional stress state of GFRP plates at the intersection or near the T-ribs. As a result, when the stress state of GFRP plates need detailed analysis, the mixed elements method (named for brevity in this paper) is a good alternative for the analysis of the structural performance of T-rib GFRP plate-concrete composite bridge decks.

3.5. Comparison of Load-Deflection Curves at Midspan Cross Section. The comparison load-deflection curves at midspan section between experiment and mixed elements method (named for brevity in this paper) of specimens GC-1, GC-2, GC-3, and and GC-4 are shown in Figure 13. It can be seen that the load-deflection curves of the mixed elements method and experiment for specimens GC-1, GC-2, GC-3, and GC-4 were basically identical before the maximum loads. After the maximum loads, the curves variations of the experiment and mixed elements method were basically consistent. Namely, the curves of the mixed elements method and experiment all presented sharp declines after the maximum loads. Therefore, it can be concluded that the mixed-dimensional FEA model proposed in this paper can accurately simulate the load-deflection curves of the GFRP plate-concrete composite bridge deck.

3.6. Comparison of Experimental Results and Simulation Results. The comparison of the predicted results of the mixed elements method (named for brevity in this paper) and experimental results for the crack loads, ultimate loads, and midspan deflection of all specimens is shown in Table 5. The ratio of experiment and prediction had a mean value of 0.986, a very small standard deviation (SD) of 0.027, and a coefficient of variation (COV) of 0.028 for ultimate loads, and corresponding values were 1.791, 0.181, and 0.101 for

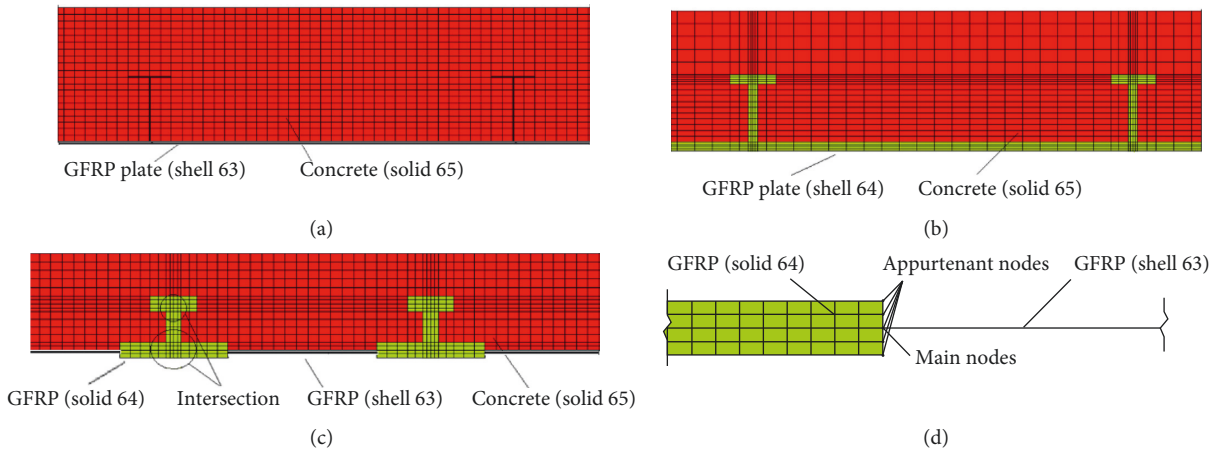

Figure 12: Three FEA modes with different methods: (a) Model I; (b) Model II; (c) Model III; (d) coupled nodes of solid and shell elements.

Table 4: Comparisons of the three different FEA modes.

Model	Number of elements of GFRP	Number of elements of concrete	Total number of elements	Computational time (min)	Global maximum stress (MPa)		Local maximum shear stress of the GFRP plate (MPa)
					Tensile	Compressive	
I	18864	113524	132388	20	37.760	33.156	—
II	138906	170624	309530	130	42.723	32.110	5.533
III	117806	125824	243630	38	40.932	31.594	5.567

crack loads, and corresponding values were 1.033, 0.058, and 0.056 for midspan deflection at the ultimate load, respectively.

It can be seen that the predictions of the mixed elements method had a good agreement with experimental results in ultimate loads and midspan deflection at the ultimate load. However, there are some discrepancies existing between predicted results and experiment results in crack loads, and the crack loads experiment values of all specimens were all bigger than predicted values. It might due to the fact that the microcracks could not timely and accurately be found in the process of increasing load; however, when the cracks were found, the microcracks already had developed a certain width.

Therefore, it can be concluded that the mixed-dimensional FEA model proposed in this paper can accurately simulate the ultimate loads and midspan deflection of the GFRP plate-concrete composite bridge deck, expect the crack loads.

4. Conclusions

The experimental study and finite element analysis of the mixed-dimensional model for the T-rib GFRP plate-concrete composite bridge decks have been presented in this paper.

(1) The test results showed that the T-rib GFRP plate-concrete composite bridge deck proposed in this paper had an excellent interface bonding performance between the concrete and GFRP plate. There was almost no slip between the concrete and GFRP plate throughout the flexural response until specimens failure occurred. The failure mode of all specimens was shear failure in concrete structures. Moreover, the strain distributions of all specimens were generally linear, and there was almost no strain redistribution caused by the interface slip.

(2) The height of concrete cross section had a significant influence on ultimate bearing capacity and stiffness of composite specimens, while the interface roughness of the GFPR plate had a slight influence on ultimate bearing capacity and stiffness of composite specimens. The longitudinal compressive reinforcing CFRP rebars had a significant influence on ductility of composite specimens, while it had a little influence on ultimate bearing capacity of composite specimens. The interface roughness of the GFRP plate and height of concrete cross section had a significant influence on crack loads of composite specimens, while the longitudinal compressive reinforcing CFRP rebars had almost no influence on crack loads of composite specimens.

(3) The mixed-dimensional FEA model proposed in this paper can accurately simulate the local complex stress state of T-ribs and GFRP plates at the intersection and simultaneously can significantly reduce computational time. The predicted and experiment results of ultimate loads, stiffness, and midspan deflection at the ultimate load all had a good consistency, expect the crack loads. Therefore,

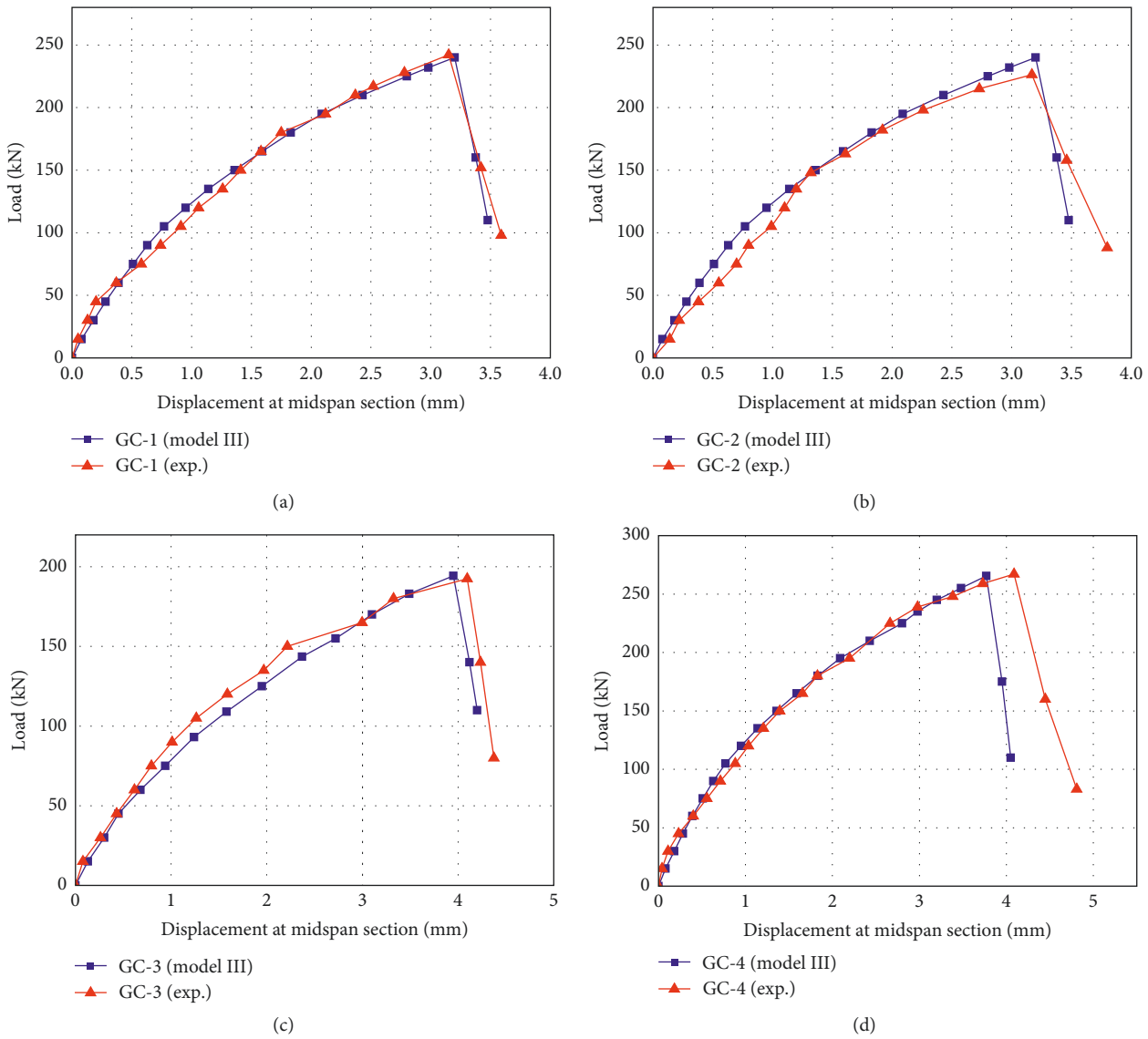

Figure 13: Comparison of the load-deflection curve at midspan cross section: (a) specimen GC-1; (b) specimen GC-2; (c) specimen GC-3; (d) specimen GC-4.

Table 5: Comparison of experimental results and predicted results of the mixed elements method.

Specimen	Load (kN)						Midspan deflection at the ultimate load (mm)		
	Crack			Ultimate					
	Experimental	Model	E/M	Experimental	Model	E/M	Experimental	Model	E/M
GC-1	55.0	31.5	1.746	242.3	240.7	1.007	3.15	3.21	0.981
GC-2	50.0	31.5	1.587	226.3	240.7	0.940	3.17	3.21	0.988
GC-3	40.0	19.2	2.083	192.5	194.3	0.991	4.10	3.95	1.038
GC-4	55.0	31.5	1.746	267.1	265.56	1.006	4.09	3.63	1.127
Mean	—	—	1.791	—	—	0.986	—	—	1.033
SD	—	—	0.181	—	—	0.027	—	—	0.058
COV	—	—	0.101	—	—	0.028	—	—	0.056

the mixed-dimensional FE analysis can provide a suitable solution to simulate the structural performance of T-rib GFRP plate-concrete composite bridge decks.

Data Availability

All data used to support the findings of this study are included within the article.

Conflicts of Interest

The authors declare that there are no conflicts of interest regarding the publication of this paper.

Acknowledgments

The authors would like to thank the National Natural Science Foundation of China (Program nos. 51809046, 51678149, and 51808562), Scientific Research Foundation for Introduce Talent by Dongguan University of Technology (GC300502-29 and GC300502-32), Guangdong Science and Technology Planning (2016A010103045), and Innovation Research Project by Department of Education of Guangdong Province (2015KTSCX141) for providing funds for this research work.

References

[1] J. Moon, M. M. Reda Taha, and J. J. Kim, "Flexural strengthening of RC slabs using a hybrid FRP-UHPC system including shear connector," *Advances in Materials Science and Engineering*, vol. 2017, Article ID 4387545, 7 pages, 2017.

[2] Z. Yang, Y. Liu, and J. Li, "Study of seismic behavior of RC beam-column joints strengthened by sprayed FRP," *Advances in Materials Science and Engineering*, vol. 2018, Article ID 3581458, 10 pages, 2018.

[3] L. Zhang, W. Liu, G. Sun, L. Wang, and L. Li, "Two-dimensional modeling of thermomechanical responses of rectangular GFRP profiles exposed to fire," *Advances in Materials Science and Engineering*, vol. 2017, Article ID 1705915, 17 pages, 2017.

[4] J. Vercher, E. Gil, Á. Mas, C. Lerma, and M. Eugenia Torner, "Flexural strengthening of damaged T-joists with severe corrosion using CFRP sheets," *Advances in Materials Science and Engineering*, vol. 2017, Article ID 6030357, 9 pages, 2017.

[5] W. T. Jung, J. S. Park, J. Y. Kang, and M. S. Keum, "Flexural behavior of concrete beam strengthened by near-surface mounted CFRP reinforcement using equivalent section model," *Advances in Materials Science and Engineering*, vol. 2017, Article ID 9180624, 16 pages, 2017.

[6] Ç. Özes and N. Neşer, "Experimental study on steel to FRP bonded lap joints in marine applications," *Advances in Materials Science and Engineering*, vol. 2015, Article ID 1642082, 6 pages, 2015.

[7] J. F. Davalos, A. Chen, and B. Zou, "Performance of a scaled FRP deck-on-steel girder bridge model with partial degree of composite action," *Engineering Structures*, vol. 40, pp. 51–63, 2012.

[8] P. J. Mendes, J. A. Barros, J. M. Sena-Cruz, and M. Taheri, "Development of a pedestrian bridge with GFRP profiles and fiber reinforced self-compacting concrete deck," *Composite Structures*, vol. 93, no. 11, pp. 2969–2982, 2011.

[9] P. H. Ziehl, M. D. Engelhardt, T. J. Fowler, F. V. Ulloa, R. D. Medlock, and E. Schell, "Design and field evaluation of hybrid FRP/reinforced concrete superstructure system," *Journal of Bridge Engineering*, vol. 14, no. 5, pp. 309–318, 2009.

[10] P. Sarir, S. L. Shen, A. Arulrajah, and S. Horpibulsuk, "Concrete wedge and coarse sand coating shear connection system in GFRP concrete composite deck," *Construction and Building Materials*, vol. 114, pp. 650–655, 2016.

[11] X. Gu, B. Yu, and M. Wu, "Experimental study of the bond performance and mechanical response of GFRP reinforced concrete," *Construction and Building Materials*, vol. 114, pp. 407–415, 2016.

[12] M. N. S. Hadi and J. Youssef, "Experimental investigation of GFRP-reinforced and GFRP-encased square concrete specimens under axial and eccentric load, and four-point bending test," *Journal of Composites for Construction*, vol. 20, no. 5, article 04016020, 2016.

[13] L. S. Sutherland, M. F. Sá, J. R. Correia, C. Guedes Soares, A. Gomes, and N. Silvestre, "Quasi-static indentation response of pedestrian bridge multicellular pultruded GFRP deck panels," *Construction and Building Materials*, vol. 118, pp. 307–318, 2016.

[14] M. Muttashar, A. Manalo, W. Karunasena, and W. Lokuge, "Flexural behaviour of multi-celled GFRP composite beams with concrete infill: experiment and theoretical analysis," *Composite Structures*, vol. 159, pp. 21–33, 2017.

[15] N. Deskovic, T. C. Triantafillou, and U. Meier, "Innovative design of FRP combined with concrete: short-term behavior," *Journal of Structural Engineering*, vol. 121, no. 7, pp. 1069–1078, 1995.

[16] L. Canning, L. Hollaway, and A. M. Thorne, "An investigation of the composite action of an FRP/concrete prismatic beam," *Construction and Building Materials*, vol. 13, no. 8, pp. 417–426, 1999.

[17] J. Hulatt, L. Hollaway, and A. Thorne, "The use of advanced polymer composites to form an economic structural unit," *Construction and Building Materials*, vol. 17, no. 1, pp. 55–68, 2003.

[18] P. Alagusundaramoorthy, I. E. Harik, and C. C. Choo, "Structural behavior of FRP composite bridge deck panels," *Journal of Bridge Engineering*, vol. 11, no. 4, pp. 384–393, 2006.

[19] A. Fam and H. Honickman, "Built-up hybrid composite box girders fabricated and tested in flexure," *Engineering Structures*, vol. 32, no. 4, pp. 1028–1037, 2010.

[20] M. Saiidi, F. Gordaninejad, and N. Wehbe, "Behavior of graphite/epoxy concrete composite beams," *Journal of Structural Engineering*, vol. 120, no. 10, pp. 2958–2976, 1994.

[21] H. Nordin and B. Täljsten, "Testing of hybrid FRP composite beams in bending," *Composites Part B: Engineering*, vol. 35, no. 1, pp. 27–33, 2004.

[22] Y. J. Kim and A. Fam, "Numerical analysis of pultruded GFRP box girders supporting adhesively-bonded concrete deck in flexure," *Engineering Structures*, vol. 33, no. 12, pp. 3527–3536, 2011.

[23] J. He, Y. Liu, A. Chen, and L. Dai, "Experimental investigation of movable hybrid GFRP and concrete bridge deck," *Construction and Building Materials*, vol. 26, no. 1, pp. 49–64, 2012.

[24] Z. Liu, P. K. Majumdar, T. E. Cousins, and J. J. Lesko, "Development and evaluation of an adhesively bonded panel-to-panel joint for a FRP bridge deck system," *Journal of Composites for Construction*, vol. 12, no. 2, pp. 224–233, 2008.

[25] T. Keller, E. Schaumann, and T. Vallée, "Flexural behavior of a hybrid FRP and lightweight concrete sandwich bridge deck," *Composites Part A: Applied Science and Manufacturing*, vol. 38, no. 3, pp. 879–889, 2007.

[26] W. Alnahhal and A. Aref, "Structural performance of hybrid fiber reinforced polymer-concrete bridge superstructure systems," *Composite Structures*, vol. 84, no. 4, pp. 319–336, 2008.

[27] J. F. Davalos, A. Chen, and B. Zou, "Stiffness and strength evaluations of a shear connection system for FRP bridge decks to steel girders," *Journal of Composites for Construction*, vol. 15, no. 3, pp. 441–450, 2010.

[28] J. R. Correia, F. A. Branco, and J. G. Ferreira, "Flexural behaviour of multi-span GFRP-concrete hybrid beams," *Engineering Structures*, vol. 31, no. 7, pp. 1369–1381, 2009.

[29] J. A. Gonilha, J. R. Correia, F. A. Branco, E. Caetano, and A. Cunha, "Modal identification of a GFRP-concrete hybrid footbridge prototype: experimental tests and analytical and numerical simulations," *Composite Structures*, vol. 106, pp. 724–733, 2013.

[30] K. Kubo, S. Ishizaki, and S. Matsui, "Development of FRP forms for composite decks," in *Proceedings of the 4th Korea-Japan Seminar on Bridge Maintenance*, Seoul, Republic of Korea, 2001.

[31] S. Y. Park, J. R. Cho, K. Cho et al., "Perfobond rib FRP shear connectors for the FRP-concrete composite deck system," in *Procedings of Fibre-Reinforced Polymers for RC Structures (FRPRCS-8)*, pp. 1–10, University of Patras, Patras, Greece, July 2007.

[32] L. Dai, "*Design and experimental study of new-type GFRP plate-concrete composite bridge decks*," M.S. thesis, Tongji University, Shanghai, China, 2009.

[33] A. Hejll, B. Täljsten, and M. Motavalli, "Large scale hybrid FRP composite girders for use in bridge structures-theory, test and field application," *Composites Part B: Engineering*, vol. 36, no. 8, pp. 573–585, 2005.

[34] J. A. Gonilha, J. R. Correia, and F. A. Branco, "Structural behaviour of a GFRP-concrete hybrid footbridge prototype: experimental tests and numerical and analytical simulations," *Engineering Structures*, vol. 60, pp. 11–22, 2014.

[35] P. A. Bakeri, "*Analysis and design of polymer composite bridge decks,*" Ph.D. thesis, Massachusetts Institute of Technology, Cambridge, MA, USA, 1989.

[36] L. Cheng, L. Zhao, V. M. Karbhari, G. A. Hegemier, and F. Seible, "Assessment of a steel-free fiber reinforced polymer-composite modular bridge system," *Journal of Structural Engineering*, vol. 131, no. 3, pp. 498–506, 2005.

[37] W. Alnahhal, A. Aref, and S. Alampalli, "Composite behavior of hybrid FRP-concrete bridge decks on steel girders," *Composite Structures*, vol. 84, no. 1, pp. 29–43, 2008.

[38] T. Guo, "*Study on mechanical performance of GFRP-concrete composite bridge decks*," M.S. thesis, Tsinghua University, Beijing, China, 2011.

[39] J. R. Correia, F. A. Branco, and J. Ferreira, "GFRP-concrete hybrid cross-sections for floors of buildings," *Engineering Structures*, vol. 31, no. 6, pp. 1331–1343, 2009.

[40] H. Nguyen, H. Mutsuyoshi, and W. Zatar, "Hybrid FRP-UHPFRC composite girders: part 1-experimental and numerical approach," *Composite Structures*, vol. 125, pp. 631–652, 2015.

[41] N. Kishi, G. Zhang, and H. Mikami, "Numerical cracking and debonding analysis of RC beams reinforced with FRP sheet," *Journal of Composites for Construction*, vol. 9, no. 6, pp. 507–514, 2005.

[42] H. Q. Cheng, D. Y. Gao, and Q. M. Zhang, "An easy method to measure the roughness of old concrete surface," *Journal of Zhengzhou University*, vol. 27, no. 1, pp. 24–26, 2006.

[43] L. Zhang, W. W. Wang, K. A. Harries, and J. Tian, "Bonding behavior of wet-bonded GFRP-concrete interface," *Journal of Composites for Construction*, vol. 19, no. 6, article 04015001, 2015.

[44] GB/T 50081-2002, *Standard for Test Method of Mechanical Properties on Ordinary Concrete*, National Standard of the People's Republic of China, Beijing, China, 2002.

[45] F. Y. Wang, Y. L. Xu, and W. L. Qu, "Mixed-dimensional finite element coupling for structural multi-scale simulation," *Finite Elements in Analysis and Design*, vol. 92, pp. 12–25, 2014.

[46] X. C. Wang, *Finite Element Method*, Tsinghua University Press, Beijing, China, 2003, ISBN 7-302-06462-8.